The Astrophysical Journal, 720:1311–1317, 2010 September 10 doi:10.1088/0004-637X/720/2/1311

MAGNETIC TRANSPORT ON THE SOLAR ATMOSPHERE BY LAMINAR AND TURBULENT AMBIPOLAR DIFFUSION

Y. Hiraki[1,3], V. Krishan[2,4], and S. Masuda[3]
[1] National Institute for Fusion Science (NIFS), Toki, Gifu, Japan; hiraki.yasutaka@nifs.ac.jp
[2] Raman Research Institute, Bangalore 560 080, India
[3] Solar-Terrestrial Environment Laboratory, Nagoya University, Nagoya, Aichi, Japan
Received 2009 August 10; accepted 2010 July 15; published 2010 August 19

ABSTRACT

The lower solar atmosphere consists of partially ionized turbulent plasmas harboring velocity field, magnetic field, and current density fluctuations. The correlations among these small-scale fluctuations give rise to large-scale flows and magnetic fields which decisively affect all transport processes. The three-fluid system consisting of electrons, ions, and neutral particles supports nonideal effects such as the Hall effect and ambipolar diffusion. Here, we study magnetic transport by the laminar- and turbulent-scale ambipolar diffusion processes using a simple model of the magnetic induction equation. Based on a linear analysis of the induction equation, we perform a one-dimensional numerical simulation to study the laminar ambipolar effect on medium-scale magnetic field structures. The nonlinearity of the laminar ambipolar diffusion creates magnetic structures with sharp gradients in the scale of hundreds of kilometers. We expect that these can be amenable to processes such as magnetic reconnection and energy release therefrom for heating and flaring of the solar plasma. Analyzing the characteristic timescales of these processes, we find that the turbulent diffusion timescale is smaller by several orders of magnitude than the laminar diffusion timescale. The effect of the modeled turbulent ambipolar diffusion on the obtained field structures is briefly discussed.

Key words: magnetohydrodynamics (MHD) – Sun: chromosphere – Sun: dynamo

1. INTRODUCTION

The generation and transport of magnetic fields, in astrophysical objects in general and in the Sun in particular, is a subject of great interest and an active area of investigation. Several variants of the mean field dynamo have been suggested for the generation and migration of the magnetic flux (Parker 1955; Moffat 1970; Stix 1972; Krause & Rädler 1980). In a partially ionized plasma, the collisions between charged particles and neutrals produce additional diffusion mechanisms such as ambipolar diffusion due to ion–neutral collisions and magnetic resistivity due to electron–neutral collisions.

The Sun is endowed with a variety of temperature variations resulting from a combination of thermal and radiative equilibria and departures therefrom. The thermal and the nonthermal nature of processes then translates into a plasma with varying degrees of ionization. Thus, the ionization fraction $\alpha = \rho_i/\rho_n$ could vary over several orders of magnitude where ρ_i and ρ_n are, respectively, the ion and the neutral hydrogen mass densities. Discrete structures such as sunspots, prominences, and spicules contain plasmas with varying degrees of ionization. The support of the neutral fluid against gravity is a major concern in the stability of these structures. Although the ideal magnetohydrodynamics (MHD) are often used as a starting point of an investigation, a partially ionized system dominated by the charged particle–neutral collisions and the neutral particle dynamics necessitates a three-fluid treatment. The strong charged particle–neutral coupling endows the neutral fluid with some of the properties of a conducting fluid. The neutral fluid is thus subjected to the Lorentz force along with the usual pressure gradient force. This attribute has been invoked to find the support for neutral component of the partially ionized cold and dense solar prominences (Leake & Arber 2006).

The evolution of the magnetic fields in such a plasma would be affected by multifluid interactions in general and ambipolar diffusion in particular (Brandenburg & Zweibel 1994; Chitre & Krishan 2001). The solar magnetic flux, generated in the convection zone, has to pass through the partially ionized solar photosphere/chromosphere before it can appear high up in the solar corona. This realization is rather recent and is now receiving a lot of attention. Arber et al. (2007) have emphasized the profound effects on the temperature and the current structure of the overlying chromosphere and the corona that an inclusion of the neutral medium can produce. It is clear that the transport and/or generation processes of the magnetic field on the solar photosphere must be studied in a partially ionized plasma. The magnetic transport would occur through laminar scale flows as well as turbulent fluctuations of the velocity field, the magnetic field, and the current density with which the photosphere is well endowed. Recently Krishan & Gangadhara (2008) have initiated the study of mean-field dynamo in a partially ionized plasma.

In this paper, we investigate magnetic transports by the flow generated by the magnetic field itself through the laminar and the turbulent ambipolar diffusions in a simplified model. The target height (500–2000 km) is between the photosphere and the corona. The horizontal scale (≈ 200 km) of our interest is comparable to or less than the scale height of the chromosphere, or a mesoscale; the scale is smaller than that of granulations (a few thousands of kilometers). The dynamics in this scale would be critical as a driver of turbulences (tens of kilometers) and be associated with various phenomena recently proposed such as chromospheric reconnections (thinning of the current sheet) and small-scale flares with a time scale of $\leqslant 1$ day. We explain briefly a three-fluid framework in Section 2. The linear analysis

[4] Honorary Professor, Indian Institute of Astrophysics, Bangalore 560 034, India.

of the laminar ambipolar diffusion of the mesoscale magnetic induction is given in Section 3.1. The fully nonlinear laminar ambipolar diffusion is studied numerically in Section 3.2. The height dependence on the magnetic structures and the correction with a non-LTE electron density distribution are mentioned in Section 4.1. We discuss the magnetic transport by turbulent ambipolar diffusion and compare its timescale with that of the laminar one in Section 4.2. In addition, we discuss the effect of the turbulent ambipolar diffusion on the magnetic structure in Section 4.3. We end the paper with a conclusion in Section 5.

For a low degree of ionization one can define a weakly ionized plasma by the condition (Alfvén & Fälthammer 1962) that the electron–neutral collision frequency $\nu_{\rm en} \sim 10^{-15} n_{\rm n} (\frac{8K_{\rm B}T}{\pi m_{\rm en}})^{0.5}$ is much larger than the electron–ion collision frequency $\nu_{\rm ei} \sim 6 \times 10^{-24} n_{\rm i} \Lambda Z^2 (K_{\rm B}T)^{-1.5}$. This translates into the ionization fraction $n_{\rm i}/n_{\rm n} < 5 \times 10^{-11}\, T^2$ where n's are the particle densities and T is the temperature in Kelvin. A major part of the solar photosphere (Krishan & Varghese 2008) qualifies as a weakly ionized plasma.

2. THREE-COMPONENT MAGNETOFLUID

We consider the three-component weakly ionized plasma consisting of electrons, ions, and neutrals with all having uniform mass densities (Krishan & Gangadhara 2008). We begin with the equation of motion of electrons including the collisional drag force by the neutral gas as $m_{\rm e} n_{\rm e} \nu_{\rm en} (V_{\rm e} - V_{\rm n})$; the electron–ion collisions have been neglected since the ionized component is of low density. On neglecting the electron inertial force, we obtain the Ohm's law for the electric field E. For timescales of interest larger than the ion–neutral collision timescale, the ion dynamics (inertial term) can also be ignored. Substituting for the form of E into the ion force balance equation, we get the relative velocity $V_{\rm n} - V_{\rm i}$ between the ions and the neutrals as a function of plasma pressure and current density J. From Faraday's law of induction along with the forms of E and $V_{\rm n} - V_{\rm i}$, we obtain the magnetic induction equation including the effect of ion–neutral collisions,

$$\frac{\partial B}{\partial t} = \nabla \times \left[\left(V_{\rm n} - \frac{J}{e n_{\rm e}} + \frac{J \times B}{c \nu_{\rm in} \rho_{\rm i}} \right) \times B \right] + \eta \nabla^2 B \quad (1)$$

where $\nu_{\rm in}$ is the ion–neutral collision frequency and $\eta = m_{\rm e} \nu_{\rm en} c^2/(4\pi e^2 n_{\rm e})$ is the electrical resistivity predominantly due to electron–neutral collisions. Note that the pressure gradient terms have been dropped for the incompressible case with constant temperature. One can easily identify the Hall term $J/en_{\rm e}$ and ambipolar diffusion term $J \times B/c\nu_{\rm in}\rho_{\rm i}$ (Chitre & Krishan 2001). The Hall term is much larger than the ambipolar term for large neutral particle densities or for $\nu_{\rm in} \gg \omega_{\rm ci}$, where $\omega_{\rm ci}$ is the ion cyclotron frequency. In this system, the magnetic field is not frozen to any of the fluids.

Substituting for the form of the relative velocity $V_{\rm n} - V_{\rm i}$ into the equation of motion of the neutral fluid, we get the equation

$$\rho_{\rm n} \left[\frac{\partial V_{\rm n}}{\partial t} + (V_{\rm n} \cdot \nabla) V_{\rm n} \right] = -\nabla p + \frac{J \times B}{c}, \quad (2)$$

where $p = p_{\rm n} + p_{\rm i} + p_{\rm e}$, the viscosity of the neutral fluid has been neglected, and $\nu_{\rm in}\rho_{\rm i} = \nu_{\rm ni}\rho_{\rm n}$ is assumed. Observe that the neutral fluid is subjected to the Lorentz force as a result of the ion–neutral coupling due to their collisions.

3. MAGNETIC TRANSPORT BY AMBIPOLAR DIFFUSION

We investigate the characteristics of the laminar ambipolar diffusion, contributing to a mesoscale magnetic transport, on the basis of theoretical and numerical approaches. In what follows, the process can be described analytically in a simple form. By performing simulations of a finite amplitude perturbation, we reproduce fine structures of magnetic fields and associated current densities through nonlinear diffusion. The motivation of this test study is to understand the ambipolar effect, and in our future studies we will perform a fully consistent simulation, including the Hall term and the neutral fluid dynamics.

3.1. Linear Analysis

In order to highlight the effect of ambipolar diffusion on magnetic transport, we ignore in the following study all other effects, i.e., the large-scale neutral fluid flow, the Hall flow, the α and β dynamo effects, and the viscosity. It is, in fact, estimated that the ambipolar term $\approx \overline{B}^2/4\pi L \nu_{\rm in}\rho_{\rm i}$ is comparable to, or larger than the Hall term $\approx c\overline{B}/4\pi L e n_{\rm e}$ at heights of 500–2000 km if the mean field $\overline{B}$ is certainly large (Singh & Krishan 2010). If the characteristic scale L is as small as ≈ 100 km, they dominate over the mean neutral flow $\overline{V}_{\rm n}$ that is assumed as $\leqslant 10^3$ cm s^{-1}; dynamo effects are negligible at the height of interest. Furthermore, we can neglect compressibility and radiative effects because the plasma pressure is decoupled from the mesoscale system in the above height range; these are necessary for the system where the ion and the neutral flow fields work.

The laminar ambipolar diffusion of the magnetic induction is described as

$$\frac{\partial \overline{B}}{\partial t} = \nabla \times \left[\frac{\overline{J} \times \overline{B}}{c \nu_{\rm in} \rho_{\rm i}} \times \overline{B} \right]. \quad (3)$$

In the local Cartesian geometry assumed for a spherical object of large radius, we choose the magnetic induction as $B = (0, B_y(x), B_z(x))$ where $B_y(x)$, $B_z(x)$ are respectively the toroidal and the poloidal components and (x, y, z) represent the latitudinal, azimuthal, and radial coordinates; we omit the bar in B. Although the physical plasma parameters such as density, temperature, and magnetic induction vary substantially along the vertical direction z, we perform here a local analysis and assume the parameters to be prescribed at a given height z. With this choice we can write the y- and the z-components of Equation (3) as

$$\frac{\partial B_y}{\partial t} = \frac{1}{a} \left(\frac{\partial B^2}{\partial x} \right) \frac{\partial B_y}{\partial x} + \frac{B_y}{a} \frac{\partial^2 B^2}{\partial x^2} \quad (4)$$

and

$$\frac{\partial B_z}{\partial t} = \frac{1}{a} \left(\frac{\partial B^2}{\partial x} \right) \frac{\partial B_z}{\partial x} + \frac{B_z}{a} \frac{\partial^2 B^2}{\partial x^2} \quad (5)$$

which can be combined as

$$\frac{\partial B^2}{\partial t} = \frac{1}{a} \left(\frac{\partial B^2}{\partial x} \right)^2 + \frac{2}{a} B^2 \frac{\partial^2 B^2}{\partial x^2}. \quad (6)$$

Here $a = 8\pi \nu_{\rm in}\rho_{\rm i}$ and $B^2 = (B_y^2 + B_z^2)$.

We first attempt a linear solution of Equation (6). Writing $B^2 = f$ and $f = f_{\rm eq} + f_1$ with $\frac{\partial f_{\rm eq}}{\partial t} = 0$ we find that the equilibrium profile is governed by the equation:

$$\frac{\partial^2 f_{\rm eq}}{\partial x^2} = -\frac{1}{2 f_{\rm eq}} \left(\frac{\partial f_{\rm eq}}{\partial x} \right)^2 \tag{7}$$

with a solution

$$f_{\rm eq}(x) = (b_1 x + b_2)^{2/3}. \tag{8}$$

As expected in the presence of ambipolar diffusion (Brandenburg & Zweibel 1994), b_1 and b_2 are the integration constants. The components of the equilibrium magnetic field can be determined by substituting for $B_{\rm eq}^2 = f_{\rm eq}$ in Equations (4) and (5). We find

$$B_{{\rm eq}y} = b_3 f_{\rm eq}^{1/2}, \; B_{{\rm eq}z} = \left(1 - b_3^2\right)^{1/2} f_{\rm eq}^{1/2}, \tag{9}$$

where b_3 is a constant. Assuming the exponential time dependence of f_1 as $\exp(\gamma t)$ we find that f_1 satisfies the second-order differential equation:

$$\frac{\partial^2 f_1}{\partial x^2} + \frac{1}{f_{\rm eq}} \frac{\partial f_{\rm eq}}{\partial x} \frac{\partial f_1}{\partial x} + \left(\frac{1}{f_{\rm eq}} \frac{\partial^2 f_{\rm eq}}{\partial x^2} - \frac{\gamma a}{2 f_{\rm eq}} \right) f_1 = 0. \tag{10}$$

By using the transformation $f_1 = f_{\rm eq}^{-1/2} g$, Equation (10) can be recast as

$$\frac{\partial^2 g}{\partial x^2} - \frac{\gamma a}{2 f_{\rm eq}} g = 0. \tag{11}$$

For a constant $f_{\rm eq}$, it describes spatially harmonic oscillations for $\gamma < 0$ with γ as the temporal damping rate, while spatially damped oscillation is described for $\gamma > 0$ with γ as the growth rate.

3.2. Simulation of Laminar Ambipolar Diffusion

From the magnetic induction Equation (3), we can determine the characteristic scales of the length L, the time T, and the magnetic field B_0 as

$$L = \sqrt{\frac{B_0^2 T}{a}} = \sqrt{\frac{1}{2} v_{\rm A}^2 T \nu_{\rm in}^{-1}}. \tag{12}$$

Note that the spatial scale depends on the time scale since we use only the induction equation, and thus L should be defined from given T and B_0. We consider the situation around a height of 1000 km on the Sun where ambipolar diffusion is important and the values of the various parameters are $B_0 = 100$ G, $\nu_{\rm in} = 2.5 \times 10^5$ s^{-1}, and $\rho_{\rm i} = 1.7 \times 10^{-13}$ g cm^{-3} (Singh & Krishan 2010). We assume $T = 21.6$ s so as to resolve the characteristic scale of the mesoscale magnetic transport (≈ 1 day), which nearly corresponds to the laminar ambipolar diffusion time $T_{\rm LA}$ (see Section 4.2). Using Equation (12), the spatial scale is estimated to be $L \approx 4.59$ km and the system size is $L_{\rm s} = 500L \approx 2300$ km. The characteristic value of the current density is found to be $j_0 = cB_0/4\pi L \approx 520$ kA.

We set the initial distribution of magnetic fields, $B_{{\rm eq}y}$ and $B_{{\rm eq}z}$, using the equilibrium solution $f_{\rm eq}$ of Equation (8) that are written as Equation (9). The field parameters are fixed as $b_1 = 10^{-3}$, $b_2 = 0.1$, and $b_3 = 0.9$. In our study, we give a perturbation only to the $B_{{\rm eq}y}$ component, representing a shear of the toroidal field introduced by vertical plasma convection. Meanwhile, the poloidal component $B_{{\rm eq}z}$, assumed to be much less than the toroidal component, is not perturbed. We perform nonlinear simulations of Equations (4)–(6) using the initial conditioning with an assumed perturbation of the Gaussian form, $C \sin(20\pi x/L_{\rm s}) \exp(-x^2/(80L)^2)$. We take two case studies with small and large initial perturbations where amplitudes are set to be $C = 0.1$ and $C = 0.5$, respectively. We adopt an Adams–Bashforth-type multistep method for time integration; the resolution is set to be $\Delta t = 4.32$ s in order to follow the Courant–Friedrichs–Lewy (CFL) stability condition. The third-order upwind biased method is used for finite differencing of the advection term. For the boundary condition at the two sides, all quantities are fixed in terms of $f_{\rm eq}$ shown just above. The current densities are calculated to be $j_y = -\frac{c}{4\pi} \frac{\partial B_z}{\partial x}$ and $j_z = \frac{c}{4\pi} \frac{\partial B_y}{\partial x}$.

Figure 1 shows latitudinal variations in the magnetic field components, B_y, B_z, and the amplitude, $|B|$, at times of $t = 0$ and 1 day in the case of small perturbation; dotted lines show the initial profiles. We find that the fluctuation in B_y decreases with time and its phase shifts slightly to the $-x$ direction by $\approx 10L$ or ≈ 45.9 km, whereas the structure with a magnitude of ≈ 10 G is produced in the B_z-component; the currents are induced with an amplitude of 2–3 kA and a latitudinal scale of 200 km. Through generation of the poloidal field, the amplitude $|B|$ is strongly relaxed to have no visible deviation from the equilibrium value $f_{\rm eq}^{1/2}$. We find that the anti-phase of B_z peaks with B_y peaks, or propagation of B_y modes, is associated with the relaxation process. These behaviors are quite similar to those in an activator–inhibitor system, or a reaction–diffusion system, and realized by the competition among B_y, B_z, and $|B|$ with different diffusion coefficients and source terms. We confirmed that similar results are obtained within a wide parameter range if C is small. Because this behavior can appear in the extreme case $B_{{\rm eq}z} \ll B_{{\rm eq}y}$, ambipolar diffusion process is important in the production of a strong poloidal field from the toroidal field.

Figure 2 shows a square of the deviation from the equilibrium magnetic field, i.e., the variable g in Equation (11) in units of $\mathrm{G}^{\frac{5}{2}}$. We compare the relaxation timescales of the linear analysis in Section 3.1 and of the nonlinear simulation results. Adopting the perturbation scale as the spatial wavenumber $k_x = 20\pi/L_{\rm s}$, the former timescale $-\gamma^{-1} = a/2 f_{\rm eq} k_x^2$ is estimated to be 1.45×10^3 s, which is exactly consistent with the latter timescale. We also find the structure resembling a sinusoidal half-mode, different from a initial Gaussian, in its fully relaxed state. The temporal variation reveals that the half-mode is formed through dissipations of higher modes as well as the amplitude itself. As the solution of Equation (11) with $\gamma < 0$, the half-mode is the lowest stable state in the fixed boundary condition with weak nonlinearity.

Figure 3 shows the distribution of magnetic fields and amplitude at $t = 54{,}000$ s in the case of large perturbation to the equilibrium profile. We clearly find that by this time intense peaks in B_y are diffused to form weak slopes and sharp troughs with different latitudinal scales. Since a large phase shift in B_y does not occur due to the fast relaxation ($\approx 10^3$ s) of fields, most of the magnetic energy is converted to B_z and its structure is characterized by the fine peaks (scales of 100 km and amplitudes of ≈ 70 G) along with broad troughs (scales of 200 km). B_z is out of phase to B_y similar to the case of small perturbation. We consider that the asymmetric feature, i.e., generation of the sharp poloidal field structure, is one of consequences of the strong nonlinear diffusion. Since the diffusion rate of a B_y

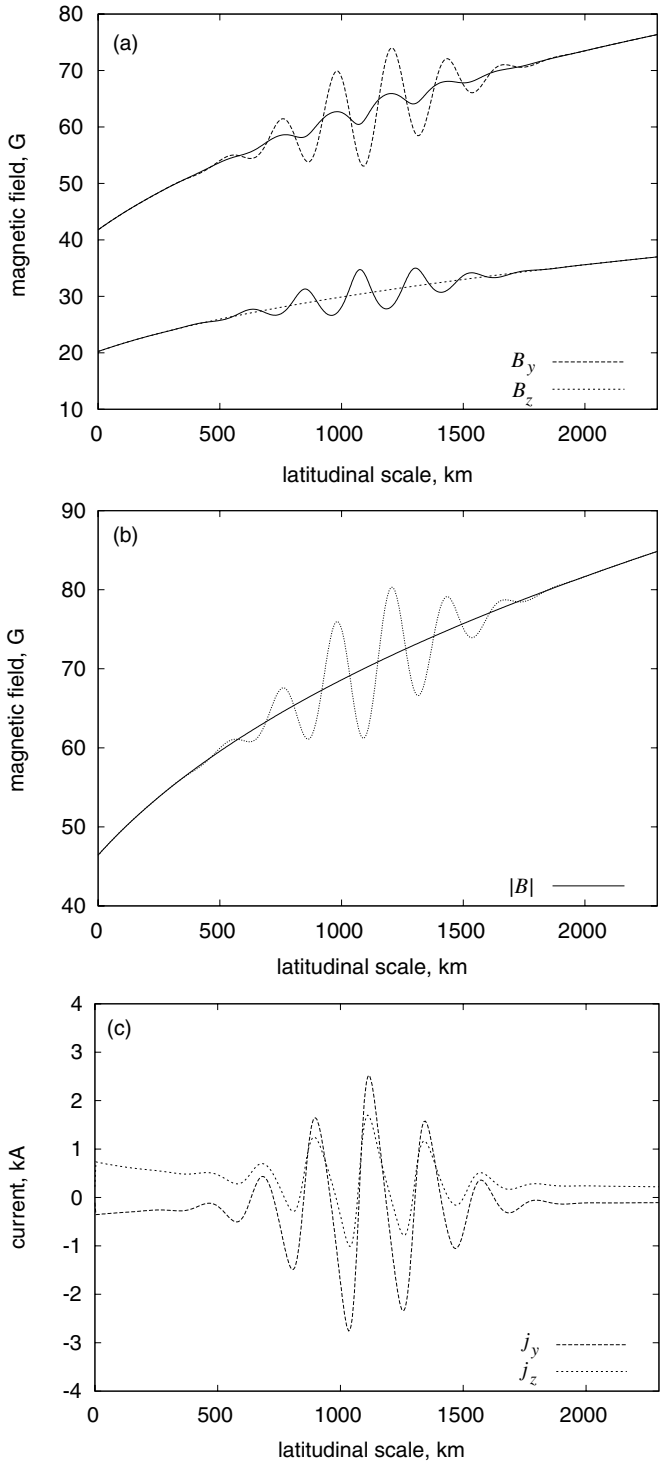

Figure 1. Latitudinal distribution of (a) magnetic fields B_y, B_z, and (b) their amplitude $|B|$ in units of G at $t = 0$ s (dotted curves) and $t = 1$ day (solid curves). As a small initial perturbation, a sinusoidal function with a Gaussian scale of $\approx$370 km and a maximum amplitude of $\approx$10 G is given to the B_y-component. The equilibrium field function is shown in the text. (c) Distribution of current densities, j_y (dashed curve) and j_z (dotted curve), in units of kA at $t = 1$ day. High currents are found to be produced at the regions where magnetic fields are condensed ($x \approx 1050$ km) as seen in panel (a).

trough at, e.g., $x \approx 1050$ km is quite slow proportional to the field amplitude $|B|$, the magnetic energy in its surroundings is converted to that in B_z through the diffusion of $|B|$. The strong and sharp currents with a maximum amplitude of 70 kA are

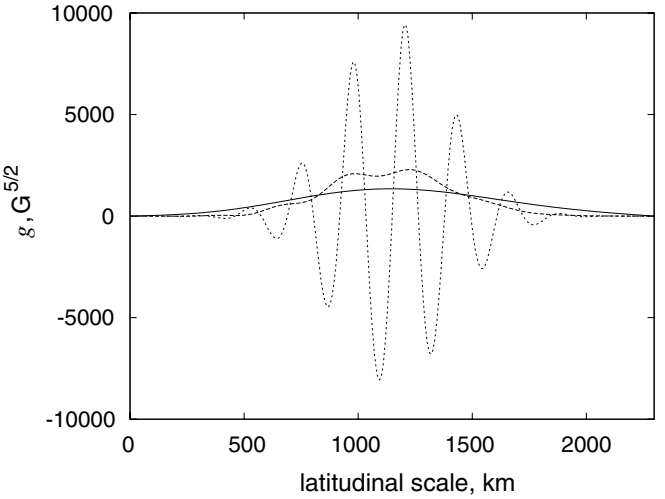

Figure 2. Temporal variation of perturbative magnetic field amplitude defined as g in units of G$^{\frac{5}{2}}$ (see the text) for the case of small perturbation. Curves with higher peaks correspond to those at $t = 0$ s, ≈ 15, 100 s, and 1 day, respectively; the latter two curves are multiplied by a factor of 50 for illustration. g is relaxed into the lowest linear harmonics $k_x = \pi/L_s$, L_s be system size.

produced at the regions where the magnetic field is condensed. Positive j_y and j_z are induced at the right edges of the troughs in B_y and the peaks in B_z; on the other hand, negative currents are induced at the right edges of the broad field areas.

We can see another feature of the strong nonlinear effect in the relaxed shape of $|B|$, which reveals a visible weak structure in Figure 3(c). In Figure 4, the shape of g is relaxed to the Gaussian profile as initially provided as an envelope. We distinguish clearly the relaxed structure from the sinusoidal half-mode of a solution of Equation (11) seen in a small perturbation case. Formation of broad slopes in B_y contributes to its formation. It is clear from these studies that nonlinear ambipolar diffusion has a large impact on the configuration of an ambient magnetic field.

4. DISCUSSION

4.1. Height Dependence on the Magnetic Transport

Neutral and ionic compositions, and their temperatures in the solar atmosphere, 500–2000 km, are known to vary strongly by several orders of magnitude. Our model formulation is still valid in a certain latitudinal scale; however, it is useful to perform a similar calculation using parameters in the other height. Figure 5 shows latitudinal distributions of the magnetic field amplitude $|B|$ for the small perturbation case at the height of 500 km and 1500 km. We readily find that the obtained behaviors of $|B|$ and the poloidal field production (B_z, not shown) are equivalent to the case in Figure 1 except for their spatial scales. This is because model Equations (4)–(6) can be normalized into dimensionless equations; the timescale is fixed as ≈ 1 day, thus the spatial scale changes according to Equation (12). Since the ion density ρ_i and the collision frequency ν_{in} decrease with height along with the magnetic field B_0, the scale of magnetic structures does not change largely with height, i.e., $\approx$400 km at $z = 500$ km and $\approx$250 km at $z = 1500$ km. However, recent numerical studies suggest that the ion density derived from a local thermal equilibrium has several orders of uncertainty (Leenaarts & Wedemeyer-Böhm 2006). Taking their calculated ionization degrees (Figure 6 in their paper), we can correct the above spatial scales to be $\approx$1300 km at $z = 500$ km and $\approx$80 km

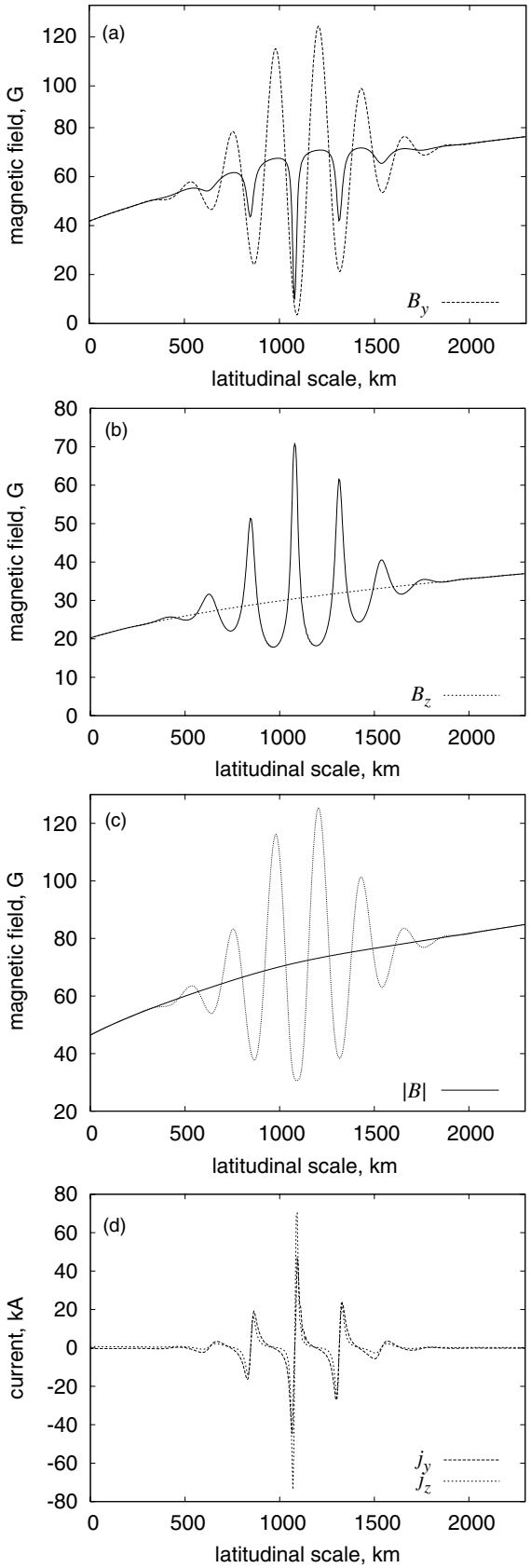

Figure 3. Similar plots as in Figure 1 but the scale and input parameters are different; (a) B_y and (b) B_z are separated for illustration, $|B|$ in panel (c) and $j_{y,z}$ in panel (d). Solid curves in panels (a)–(c) show the values at $t = 54{,}000$ s, while dotted show initial values. For the study of strong nonlinearity, a large amplitude of initial perturbation (≈ 60 G in maximum) is provided. In panel (d), higher currents (≈ 70 kA) are produced at $x \approx 1050$ km compared with a small perturbation case.

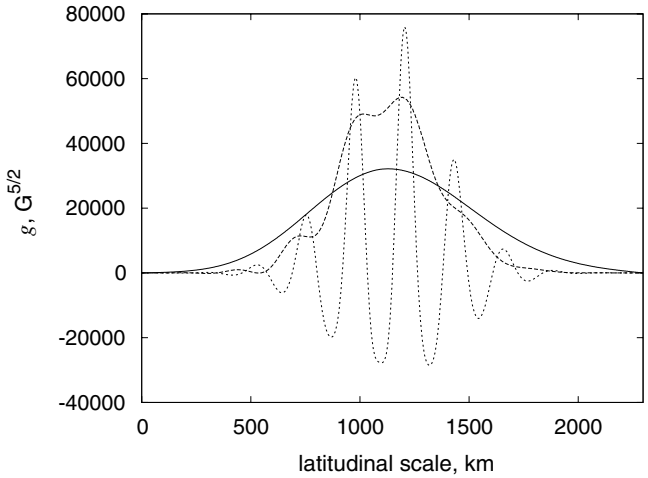

Figure 4. Similar plots as in Figure 2 but for the case of large field perturbation. Curves with higher peaks correspond to those at $t = 0$ s, ≈ 8640 s, and 54,000 s, respectively; the latter two curves are multiplied by a factor of 20 for illustration. g is relaxed into a Gaussian form similar to the initial perturbation.

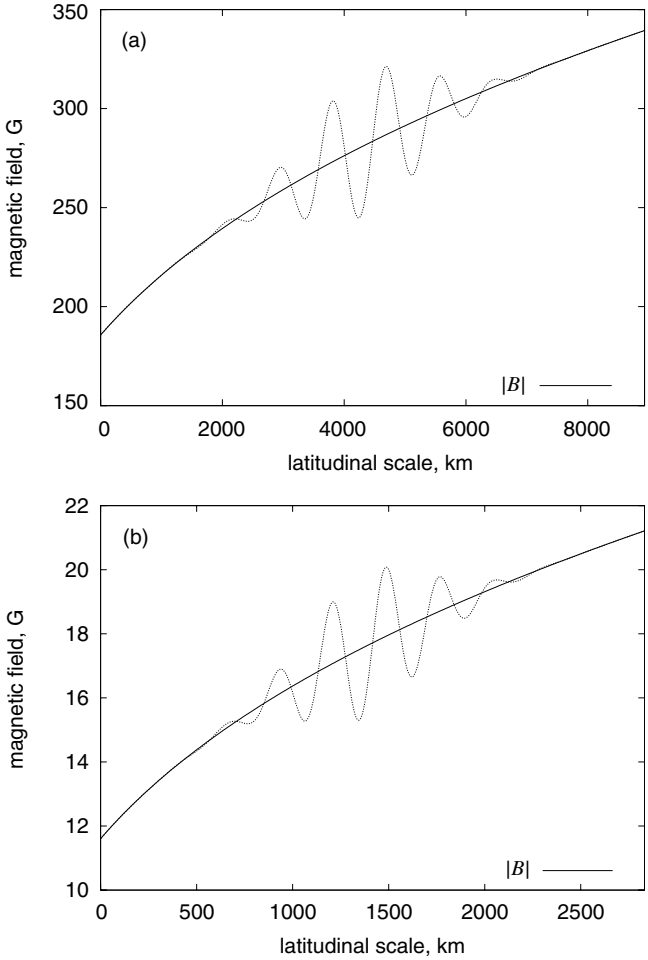

Figure 5. Magnetic field amplitudes $|B|$ in units of G at $t = 0$ s (dotted curves) and $t = 1$ day (solid curves) for the case of small perturbation; the plasma parameters at a height of (a) 500 km and (b) 1500 km are used.

at $z = 1500$ km, whereas it remains unchanged to be ≈ 200 km at $z = 1000$ km. Thus, the magnetic field structure becomes small with an increase in height. Considering expansion of a magnetic flux tube, ambipolar diffusion seems to be effective in the lower height.

4.2. Timescale Analysis on Turbulent and Laminar Ambipolar Diffusions

One way of studying turbulence in a system is by splitting the physical quantities into small-scale and large-scale parts. Following the standard procedure of the mean-field dynamo (Krause & Rädler 1980), the velocity $V_n - J/en_e + J \times B/c\nu_{in}\rho_i$ and the magnetic field B are split into their average large-scale parts as $\overline{B}$ and the fluctuating small-scale parts as B'. Applying this theory to the magnetic induction equation, the temporal variation in the mean field $\overline{B}$ is obtained as the zeroth-order component. Ambipolar diffusion consists of two terms, the first of which represents the laminar component $\sim (\overline{J} \times \overline{B}) \times \overline{B}$ seen in Equation (3), while the second term represents the turbulent process $\sim (\overline{J' \times B'}) \times \overline{B}$. Here, we point out the importance of the turbulent ambipolar diffusion by comparing its timescale with the laminar process using a fluctuating field analysis. The laminar and the turbulent ambipolar diffusions of the magnetic induction are described as

$$\frac{\partial \overline{B}}{\partial t} = \nabla \times \left[\frac{\overline{J} \times \overline{B}}{c\nu_{in}\rho_i} \times \overline{B} + \frac{\overline{J' \times B'}}{c\nu_{in}\rho_i} \times \overline{B} \right]. \quad (13)$$

We estimate the second term as follows:

$$\overline{J' \times B'} = \overline{\frac{-\nabla B'^2}{8\pi c} + \frac{B' \cdot \nabla B'}{4\pi c}}. \quad (14)$$

The left-hand side is the average Lorentz force due to magnetic fluctuations and we assume that it is nonzero. On the right-hand side, the first term is symptomatic of the turbulent magnetic pressure and the second is the contribution to the turbulent curvature. If magnetic fluctuations are introduced in a fluid initially at rest, the Lorentz force will drive motion in the fluid. In an incompressible fluid, the direction of the flow is along the predominant component of the fluctuating field. This arises through the curvature term $B' \cdot \nabla B'$ since only the solenoidal part of the Lorentz force can drive flows in an incompressible fluid or in a compressible fluid under the Boussinesq approximation as discussed by Ogilvie (2003). The gradient part of the Lorentz force is compensated for by the pressure gradient. Here, we shall make an approximate estimate of this term as

$$\overline{J' \times B'} \approx \frac{c}{4\pi\lambda_{cor}} \overline{B'^2}, \quad (15)$$

where λ_{cor} is the correlation length of the magnetic fluctuations.

We follow Krause & Rädler (1980) in order to estimate the mean square of the magnetic fluctuations $\overline{B'^2}$. In the high conductivity limit ($\eta \approx 0$), the fluctuation B' is produced by the interaction of the turbulent velocity field V'_E with the mean magnetic field $\overline{B}$ over a time scale τ_{cor}, where τ_{cor} is the correlation timescale of the fluctuating fields. Thus, the elemental field B'_{el} is given by

$$B'_{el} \approx \frac{V'_E \tau_{cor}}{\lambda_{cor}} \overline{B}. \quad (16)$$

After a time interval τ_{cor} the turbulent field V'_E changes nearly completely. This new realization of the turbulent V'_E interacts with $\overline{B}$ to produce another elemental field B'_{el} uncorrelated with the previous field element. Each field element survives over the dissipation time scale $\tau_{dis} \approx \lambda^2_{cor}/\eta$ much larger than the correlation time τ_{cor}. Thus, the total fluctuating field B' is the incoherent sum of these elemental fields B'_{el}. The number n of these elemental fields is given by

$$n \approx \frac{\tau_{dis}}{\tau_{cor}} = \frac{\lambda^2_{cor}}{\eta\tau_{cor}}. \quad (17)$$

Thus, to the order of magnitude, B' is found to be

$$B' \approx \sqrt{n} B'_{el} \approx \sqrt{\frac{V'^2_E \tau_{cor}}{\eta}} \overline{B}. \quad (18)$$

And

$$\overline{B'^2} \approx R_M S \overline{B}^2 \quad (19)$$

where

$$R_M = \frac{\langle V'_E \rangle \lambda_{cor}}{\eta}, \qquad S = \frac{\langle V'_E \rangle \tau_{cor}}{\lambda_{cor}} \quad (20)$$

are respectively the magnetic Reynolds number and the Strouhal number; rms of V'_E is denoted as $\langle \cdot \rangle$.

We can now estimate the time scales of the laminar ambipolar diffusion, T_{LA} and the turbulent ambipolar diffusion, T_{TA} from the magnetic transport Equations (13) as

$$T_{LA} \approx \frac{4\pi \overline{L}^2 \rho_i \nu_{in}}{\overline{B}^2}, \qquad T_{TA} \approx \frac{4\pi \overline{L} \lambda_{cor} \rho_i \nu_{in}}{\overline{B'^2}}, \quad (21)$$

where $\overline{L}$ is the characteristic spatial scale associated with the mean magnetic field $\overline{B}$. Substituting from Equation (20), we find the ratio of the two timescales to be

$$\frac{T_{TA}}{T_{LA}} = (R_M S)^{-1} \frac{\lambda_{cor}}{\overline{L}}. \quad (22)$$

Now the magnetic Reynolds number $R_M \gg 1$, the Strouhal number $S < 1$ and the correlation length $\lambda_{cor} \ll \overline{L}$; therefore, the turbulent ambipolar diffusion timescale T_{TA} can be much smaller than the laminar ambipolar diffusion timescale T_{LA}. This is exactly what is expected of a turbulent transport process. The reason for the greater efficiency of a turbulent transport over a laminar transport is that in a turbulent process a physical attribute on a mesoscale is transferred to a small scale and it is much easier for a small-scale quantity to diffuse than for a mesoscale one to diffuse. For the typical values of the physical parameters at a height of interest (see Section 3.2, $\overline{L} \approx$ 100–200 km in Figures 1 and 3), we find $T_{LA} \approx 10^4$ s, $\leqslant$1 day, and T_{TA} could be smaller by several orders of magnitude.

4.3. The Effects of the Turbulent Diffusion

In this section, we first assess the effect of turbulent ambipolar diffusion on the mesoscopic magnetic structures provided in Section 3.2. We tried to perform a test simulation including the modeled turbulent effect; the details are shown below. Second, we point out some contributions of ambipolar diffusion to observed fine structures in the solar atmosphere.

In Section 4.2, we evaluated the magnitude of the turbulent diffusion timescale, T_{TA}, and found the relation $T_{TA}/T_{LA} = \varepsilon$ as Equation (22); ε is a small parameter. Using Equations (15) and (19), we can write the magnitude of the turbulent Lorentz force as $4\pi|\overline{J' \times B'}|/c \approx \overline{B'^2}/\lambda_{cor} = \overline{B}^2/\varepsilon L$. As the curvature term is predominant in Equation (14), this force points parallel to the fluctuating field B'. However, we cannot solve the fluctuating

field B' self-consistently with the mean field $\overline{B}$. We assume here that the direction of the turbulent field, $\xi(x)$, changes temporarily, while its long-time average meets the relation $\langle\xi(x)\rangle = 0$; that is, the turbulence is isotropic. For numerical convenience, we define the value as $-1 \leqslant \xi \leqslant 1$ for each spatial point using a uniform random number; we assign the same value of ξ between the time scale of $\lambda_{\rm cor}$. Thus, we can write the turbulent ambipolar term in Equation (13) as $-\frac{\partial}{\partial x}\overline{B}^2\xi \times \overline{B}/8\pi\nu_{\rm in}\rho_{\rm i}\varepsilon$ where we convert $1/L$ to $\frac{\partial}{\partial x}$ not to change the form of the diffusion equation. Operating $\nabla\times$, we get the y- and z-components of the term as $\frac{1}{\varepsilon a}\frac{\partial}{\partial x}(\frac{\partial B^2}{\partial x}\xi B_y, \frac{\partial B^2}{\partial x}\xi B_z)$ and solve Equations (4)–(6) by adding this turbulent effect; ε is assumed to be 0.1.

We see the temporal variation in magnetic fields for which most parameters are set to be the same as the small perturbation case in Section 3.2. For numerical efficiency, we set the system size $L_{\rm s} = 46$ km and the resolution $\Delta x = 0.046$ km. At the very initial phase, the peaks in B_z become pointed and produce some new peaks with a small spatial scale $\lambda_{\rm cor} \approx 0.5$ km. We also find that a strong current is induced at the steep gradient of the field. However, we cannot reproduce the further time variation, suffering from numerical oscillations; this is because ξ defined by a random number is not appropriate for fluid simulation. We should renormalize the turbulent effect to be treated successfully in the laminar scale and will study the produced magnetic structures through the interaction of these scales. Another important effect of turbulent ambipolar diffusion is to transport magnetic energy in the radial direction. Similar to molecular diffusion, local enhancement of the energy in the lower atmosphere ($\approx$500 km) leads to its systematic increase up to $\geqslant$1000 km with a certain scale height. Based on our timescale analysis, the transport of a strong magnetic shear, or a thin current sheet, can be realized on a very short timescale (e.g., $t \approx$ 100–200 s).

We briefly mention a possible role of the ambipolar diffusion process implied in some observable atmospheric phenomena. For the last few decades, magnetic reconnection in partially ionized plasma with ambipolar and Hall effects has been analyzed (see Krishan 2009, and references therein). The evidence for chromospheric reconnection is clearly found from recent satellite observations such as a large number of fine (highly convective) structures in the vicinity of sunspots. In our previous study, the slab scale and the formation speed of the Sweet–Parker-type current sheet are estimated with a simple analysis of the induction equation in the MHD regime. This study presents a nonlinear analysis of the ambipolar effect, which results in the formation of thin current sheets with a mesoscale $\leqslant$100 km and a short time scale of 10^3 s. Since the scale is close to the kinematic regime, we point out the importance of turbulent ambipolar diffusion in the further thinning process of the current sheets. We expect that nonlinear ambipolar diffusion works as one of the mechanisms sustaining observed fine structures through radial magnetic transport from the chromosphere.

5. CONCLUSION

We find that ambipolar diffusion is an important effect in the partially ionized part of the solar atmosphere. The laminar ambipolar transport is found to create magnetic structures with steep gradients in a horizontal scale of 100–200 km. The turbulent part of ambipolar diffusion could transport these structures on a timescale which could be shorter by orders of magnitude than all the other processes. Thus, the formation and migration of magnetic structures to higher up in the solar atmosphere could be the result of ambipolar diffusion.

Y.H. thanks the Raman Research Institute (Bangalore, India) for supporting his visit during which a part of this work was done. Another part was done during V.K.'s stay as a visiting professor at the Solar-Terrestrial Environment Laboratory (STEL) of Nagoya University.

REFERENCES

Alfvén, H., & Fälthammer, C.-G. 1962, Cosmic Electrodynamics (Oxford: Clarendon)
Arber, T. D., Haynes, M., & Leake, J. E. 2007, ApJ, 666, 541
Brandenburg, A., & Zweibel, E. G. 1994, ApJ, 427, L91
Chitre, S. M., & Krishan, V. 2001, MNRAS, 323, L23
Krause, F., & Rädler, K.-H. 1980, Mean-Field Magnetohydrodynamics and Dynamo Theory (Oxford: Pergamon)
Krishan, V. 2009, MNRAS, 400, 2200
Krishan, V., & Gangadhara, R. T. 2008, MNRAS, 385, 849
Krishan, V., & Varghese, A. B. 2008, Solar Phys., 247, 343
Leake, J. E., & Arber, T. D. 2006, A&A, 450, 805
Leenaarts, J., & Wedemeyer-Böhm, S. 2006, A&A, 460, 301
Moffat, H. K. 1970, J. Fluid Mech., 41, 435
Ogilvie, G. I. 2003, MNRAS, 340, 969
Parker, E. N. 1955, ApJ, 122, 293
Singh, K. A. P., & Krishan, V. 2010, New Astron., 15, 119
Stix, M. 1972, A&A, 20, 9